In: AIAA SciTech Forum 2023, 23-27 January 2023, National Harbor, Maryland
DOI: 10.2514/6.2023-2242

Robust Multi-Sensor Navigation in GNSS Degraded Environments

G. Villalobos [1], I. Petrunin [2] and H.-S. Shin [3]
Cranfield University School of Aerospace Transport and Manufacturing, Cranfield, Central Bedfordshire, MK43 0AL, United Kingdom.

J. Gilmour[4]
Leonardo Helicopters, Yeovil, Somerset, United Kingdom

The success of an Unmanned Aircraft Vehicle for effective operation beyond visual line of sight is linked to the system's ability to maintain precise positioning during stationary and maneuvering flight under all encountered conditions, such as sensor measurement degradation or unavailability. Therefore, unmanned operations demand a resilient, accurate, and integral navigation system. Sensor fusion increases data redundancy by combining measurements from complementary sensors, such as Global Navigation Satellite Systems GNSS, Visual Inertial Navigation Systems VINS, and Light Detection and Ranging Systems LIDAR. This research aims to propose an enhanced adaptative sensor switching mechanism within a multi-sensor navigation system for improved robustness in GNSS-degraded environments accounting for accuracy through the interaction between different sensor models by means of their probability of failure. The switching is driven by a real-time process that dynamically adapts to sensor loss and degradation environments based solely on each sensor's adaptative probability of failure and their interaction. This approach is developed based on previous research and is improved to account for the dependency of heuristic determination for sensor uncertainty models. The simulation is achieved with the help of the UAV Toolbox from MATLAB and the positioning signals modeled through ground truth manipulation with existing error models to test and evaluate the proposed methodology. The results presented show an improvement by mitigating the heuristic dependency and Markov chain sensitivity reported in previous research.

I. Nomenclature

DUU	=	Dynamic Uncertainty Update
EPU	=	Estimated Position Uncertainty
GNSS	=	Global Navigation Satellite System
HMI	=	Hazardous Misleading Information
IMM	=	Interactive Multiple Model filter
IMU	=	Inertial Measurement Unit
LIDAR	=	Light Detection and Ranging
LIO	=	Lidar Inertial Odometry
RMSE	=	Root Mean Square Error
SOPs	=	Signals of Opportunity
UAV	=	Unmanned Aerial Vehicle

[1] MSc Graduate, Cranfield University School of Aerospace Transport and Manufacturing, Cranfield, United Kingdom
[2] Senior Lecturer, Cranfield University School of Aerospace Transport and Manufacturing, Cranfield, United Kingdom.
[3] Professor, Cranfield University Cranfield School of Aerospace Transport and Manufacturing, Cranfield, United Kingdom.
[4] Technical Team Lead, Flight Control Systems UK, Leonardo Helicopters, Yeovil, Somerset, United Kingdom.

Published by AIAA. This is the Author Accepted Manuscript issued with: Creative Commons Attribution Non-Commercial License (CC:BY:NC 4.0).
The final published version (version of record) is available online at DOI:10.2514/6.2023-2242. Please refer to any applicable publisher terms of use.

UGV = Unmanned Ground Vehicle
VINS = Visual Inertial Navigation Systems
VIO = Visual Inertial Odometry

II. Introduction

Autonomous vehicles are currently the focal point for a huge variety of industries. The sociological and economic effects of incorporating these vehicles into our lives—from Unmanned Ground Vehicles (UGVs) to Unmanned Aerial Vehicles (UAVs)—are amazing. The demands on these vehicles' navigation systems are becoming more and more challenging as we give them increased levels of autonomy. Therefore, failures in the navigation system can lead to disastrous results [1]. Consequently, the navigation system demands an accurate, resilient, and integral positioning estimation at any time under any environment.

Due to static infrastructures, such as buildings and dense vegetation, dynamic barriers, such as traffic, pedestrians, and environmental factors, such as shadows, sunshine, and weather, vehicles operating in urban settings confront issues. Reduced satellite visibility in metropolitan areas, for Global Navigation Satellite System (GNSS) devices, fewer readings are obtained in the best-case scenario, while in the worst-case scenario, the signal is completely blocked. Additionally, these technologies encounter satellite problems brought on by multipath received signal flaws, in addition to several extra sources of inaccuracy from the ionosphere and clock offsets, while the low GNSS transmission power makes it a vulnerable target for intentional jamming or spoofing attacks [2]. Therefore, to guarantee end-to-end positioning systems, the alternative non-GNSS navigation source must reach a level of operational readiness that enables it to be used resiliently. This means that it must be able to not only detect when any of the failure modes are present but also to ensure the integrity of navigation in their presence, as well as self-correct and recover from such failures, all in an autonomous, real-time architecture [3].

In order to solve this problem, several sensor fusion and management architectures have been created to facilitate all source navigation. For this, currently, a transition matrix Markov chain is used to define the ideal weight to each sensor for the total system position estimation. However, this technique is based on a heuristic determination that must be updated for each navigation environment that the vehicle faces, which is not suitable for unmanned navigation.

This paper aims to propose and investigate a dynamic uncertainty update for a multi-sensor interactive sensor switching method for UAV navigation in GNSS-degraded environments that autonomously manages available and faulty sensors while delivering an accurate positioning signal from the whole system despite sensor failures. For this purpose, a multi-sensor fusion architecture is proposed based on previous research, where each of the system's component modules performs a specific function contributing directly to achieving integral and resilient navigation, consisting of the following modules: integrity monitoring, fault detection, independent filters, main fusion, and the proposed dynamic uncertainty update.

III. Related Work

Distributed efforts have been suggested to develop sensor fusion architectures that ensure system integrity by monitoring faults, isolating them, and evaluating the entire system's performance against hazardous misleading information (HMI) unacceptable to human safety, leading to a research gap in their integration. Cheng [4] suggests an all-in-one solution for a multi-sensor fusion system as a result. The Resilient Interactive Sensor-Independent-Update Fusion namely ISIU methodology, attempts to incorporate the Interactive Multiple Model filter (IMM) structure as a multi-sensor fusion core for a system architecture capable of recognizing and mitigating its own faults while the integrity of the entire system is monitored.

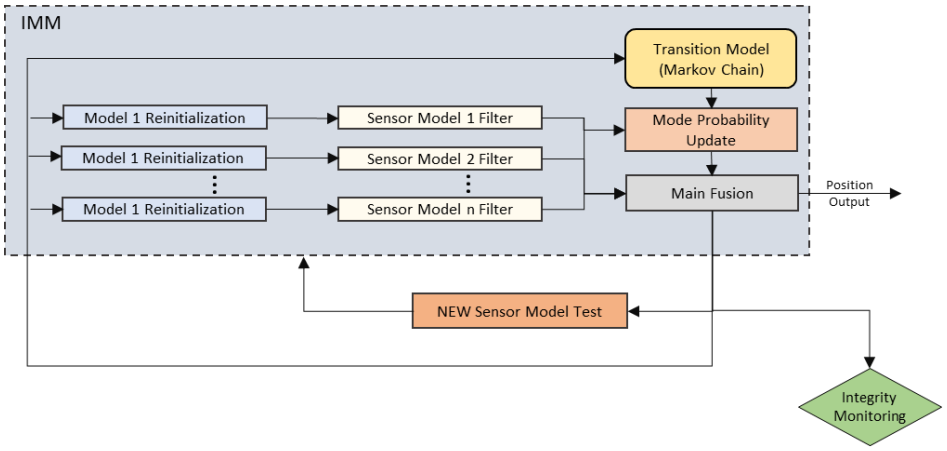


Figure 1. Resilient Interactive Sensor-Independent-Update Fusion methodology, an overview of the principal modules readapted from [4]**.**

IMU, GNSS, LIDAR, and Camera are integrated by ISIU to demonstrate the notion of its architecture. IMU is then loosely coupled to each observation sensor (GNSS, LIDAR, and Camera) employing the Error State Kalman Filter (ESKF), which it uses as the independent filter for the sensor models *1,2…n*.

A fixed Markov Chain is employed to define the transition probability between the sensor models (IMU/GNSS, IMU/LIDAR, and IMU/Camera), which is the main drawback of the technique. For each unique circumstance, this matrix must be heuristically updated. For instance, the GNSS sensor should be given less credibility in the event of an urban deep canyon and higher credibility for LIDAR and visual sensors, making it an undesirable choice for autonomous systems.

IV. Proposed Solution

A. Sensor selection

First of all, to select the best system's sensor models, an in-depth literature review was carried out comparing positioning techniques used for GNSS-denied navigation, as a result, a selection of the most accurate positioning sensors and technics is shown in Figure 2. The accuracy assessment for this work is accepted as the RMSE measured in all the research papers by comparing with a ground truth reference obtained through RTK technologies and, in some cases, consumer-grade GNSS/IMU sensors.

According to the data, LIDAR odometry and Visual odometry-related technologies, LIDAR/IMU and LIDAR/Stereo Camera/IMU, are on top of the accurate positioning technologies for urban air mobility achieving sub-meter results. The second-best pair of technologies relates to SOPs with carrier phase measurements of 3G and 4G signals. It is critical to highlight the regulated environment in which the 3G and 4G tests were performed since this accuracy level is only achieved under conditions where the UAV stays inside the same BTs and eNB areas (120deg). Fly-past these areas can lead to errors of dozens of meters and is still a research topic [5].

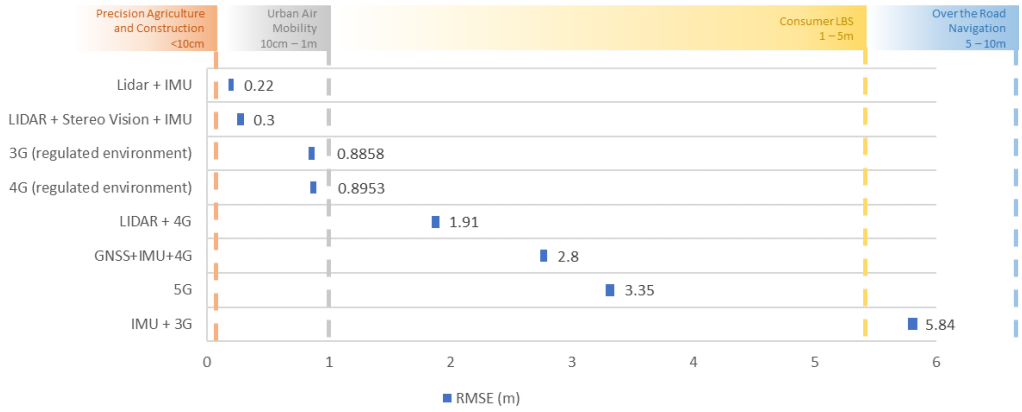


Figure 2. Comparison summary of recent positioning technics for GNSS denied navigation [5]–[11]. For the convenience of the accuracy classification, the illustration adapts the standard developed in the report to congress from Homeland Security of the U.S. [12].

Based on the information, the selected positioning technics were VIO, LIO, and GNSS/IMU, to be included in the architecture in order to analyze the system for a multi-sensor fusion configuration.

B. System Architecture

The proposed system architecture features the incorporation of a Dynamic Uncertainty Update (DUU) segment responsible for updating the uncertainty of the sensor fidelity prior to the main fusion. Figure 3 depicts the proposed framework, and Figure 1 makes it simple to spot the key distinctions from earlier studies.

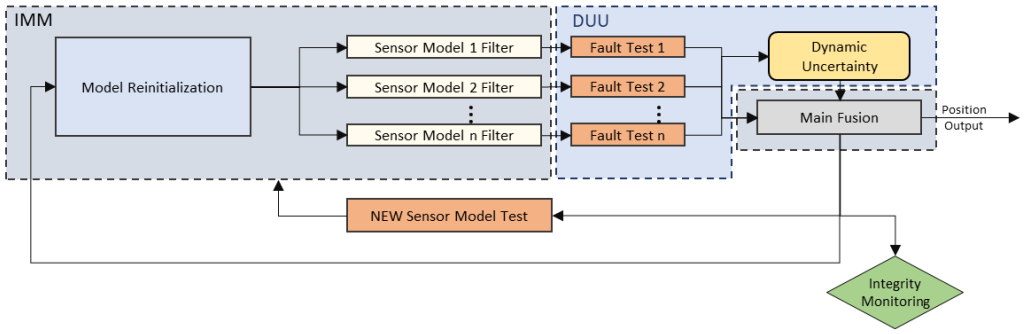


Figure 3. The system architecture of the proposed sensor fusion architecture with the state-of-the-art Dynamic Uncertainty Update (DUU) section. Every color represents different modules of the comprehensive architecture, while dashed lines represent the two main segments of the IMM adapted filter and DUU.

The modules conforming to the architecture are Model Reinitialization, Sensor Model Filters, Fault Detection and Exclusion, Dynamic Uncertainty Update, Main Fusion, and Integrity Monitoring. It is of utmost importance to highlight a major difference with the ISIU methodology, for the independent sensor model filters, this work employs full-state Kalman filters with a kinematic model of the UAV to predict the measurements for the individual sensor models in contrast with ISIU, which uses error state Extended Kalman filters with an IMU sensor model to predict the measurements. Therefore, the developed architecture relies on the vehicle model, comparing kinematic data with actual sensor measurements, while ISIU compares IMU measurement estimation data with sensor measurements.

C. Dynamic Uncertainty Update

The main knowledge contribution of this work lies in the development of an interaction module to provide the system with adaptability to environments where the failure of one or more sensors, in this case, GNSS, prevails since, as mentioned in section III. the ISIU method lacks autonomy due to the heuristic determination of the Markov chain

probability matrix. For fixed Markov chains, the probability of a one-step transition does not change with time, and the one-step transition probability must hold the following conditions:

$$p_{ji} \geq 0\,, \quad \sum_{i} p_{ji} = 1 \tag{1}$$

Where the transition probabilities are represented as:

$$p_{ji} = \begin{bmatrix} p_{11} & p_{12} & \cdots & p_{1j} \\ p_{21} & p_{22} & \cdots & p_{2j} \\ \vdots & \vdots & \vdots & \vdots \\ p_{\mathrm{i}1} & p_{i2} & \cdots & p_{ij} \end{bmatrix} \tag{2}$$

The essential component of the adaptative transition matrix is the evaluation of the mode probability gradient to determine the variation of the weights assigned to the *i*th independent filter; this procedure is based on [13], [14]. The result is calculated by comparing the predicted mode transition probability with the updated mode transition probability and can be computed as follows:

$$\Delta\mu_{k/k}^{(i)} = \mu_{k/k}^{(i)} - \mu_{k-1/k-1}^{(i)} \tag{3}$$

The mode transition probability estimation, also named mixing weights linked from the reinitialization module, is calculated by:

$$\mu_{k/k}^{(j)|(i)} = \frac{p_{ji}\mu_{k-1/k-1}^{(i)}}{\mu_{k/k-1}^{(i)}} \quad i,j = 1,\ldots,r \tag{4}$$

Where r stands for the number of sensor models (independent filters). The predicted mode transition probability for the following epoch is computed as

$$\mu_{k/k-1}^{(i)} = \sum_{\mathrm{i}=1}^{r} p_{ji}\mu_{k/k}^{(\mathrm{i})} \tag{5}$$

And the mode transition probability update $\mu_{k/k}^{(i)}$ associated with the main fusion module is

$$\mu_{k/k}^{(i)} = \frac{\mu_{k/k-1}^{(i)} L_k^{(i)}}{\sum_{\mathrm{i}=1}^{r} \mu_{k/k-1}^{(j)} L_k^{(j)}} \tag{6}$$

By introducing the mode likelihood that can be calculated for each independent filter with

$$L_k^{(i)} = \frac{1}{\sqrt{\det\left(2\pi \mathrm{S}_k^{(i)}\right)}} \exp\left[-\frac{1}{2}\tilde{\mathrm{Z}}_k^{(i)\mathrm{T}} \mathrm{S}_k^{(i)-1} \tilde{\mathrm{Z}}_k^{(i)}\right] \tag{7}$$

Where $\mathrm{S}_k^{(i)}$ and $\tilde{\mathrm{Z}}_k^{(i)}$ refer to the covariance and measurement innovations from the ith sensor model independent filter. Then a function is specified to correct the gradient values

$$f_{k/k}^{(i)} = \frac{1}{1 - \Delta\mu_{k/k}^{(i)\mathrm{T}}} \tag{8}$$

to subsequently correct the Markov Chain with the corrected gradients

$$p_{ji_{k/k}}{}' = f_{k/k}^{(i)} * p_{ji_{k-1/k-1}} \tag{9}$$

and finally, normalize the values of the transition probability

$$p_{ji_{k/k}} = \frac{p_{ji_{k/k}}{}'}{\sum_{i=1}^{r} p_{ji_{k/k}}{}'} \tag{10}$$

In these equations, the data from the previous model is included in the transition probabilities after being modified by the transition probability correction function. The probability of the model *i* is increasing when $\Delta\mu_{k/k}^{(i)} > 0$ and $f_{k/k}^{(i)} > 1$. Consequently, after normalization, $p_{ji_{k/k}} > p_{ji_{k-1/k-1}}$, indicating that the transition probability from other models to the model *i* is higher. While in the opposite case $\Delta\mu_{k/k}^{(i)} < 0,\ f_{k/k}^{(i)} < 1$ the transition probability $p_{ji_{k/k}} < p_{ji_{k-1/k-1}}$ suggesting that the probability of transition from other models to model *i* decreases. The procedure can be verified as

it maintains the condition from equation (1) for a one-step transition fixed Markov chain at all times, therefore the initial values $p_{ji_{0/0}}$ must be set following the same condition, otherwise, errors can be derived.

V. Results and Discussion

D. Simulation

Simulation is carried out using Matlab/Simulink with the incorporation of the UAV toolbox to simulate a low-fidelity dynamic quadrotor model featuring position controllers to follow a defined set of 3D waypoints to provide realism to the vehicle's actuation. In order to simulate VIO, LIO and GNSS/IMU positioning measurements, the following error models commonly presented in multi-sensor navigation systems were implemented according to [15] as follows:

Table 1. Error models for positioning measurements

Positioning	Error model	Error model	Notation
GNSS/IMU	Step error	$E(t) = Au(t - t_0)$	A, fault magnitude, $u(t)$, unit step function after the initial failure time t_0.
	Random walk	$E(t) = \frac{a(t)}{\sqrt{dt}} u(t - t_0)$	$a(t)$, random variable with gaussian statistical distribution, $u(t)$, unit step function after the initial failure time t_0.
VIO	Incremental drift	$E(t) = \frac{1}{2}\varpi t^2$	ϖ, position error factor in each X, Y and Z component.
LIO	Random walk	$E(t) = \frac{a(t)}{\sqrt{dt}} u(t - t_0)$	A, fault magnitude, $u(t)$, unit step function after the initial fault time t_0.

Figure 4 displays the GNSS degraded environment simulation results. The GNSS/IMU position carries a horizontal and vertical random walk noise with a standard deviation of *3 m*, featuring two injected step errors of *6 m* bias and a third one of *– 8 m* at *t = 10, 25,* and *41 seconds* with a duration of *2.2, 2.7* and *1.1* seconds, respectively. VIO signal features an incremental drift with a position error factor of ϖ *= [0.003,0.003.0.001] m,* while LIO only keeps a horizontal and vertical random walk noise with a standard deviation of *0.6* and *0.2 m*. Table 2 features the absolute RMSE from each position measurement, supported by the experiments of [10], [16], where for LIO, sub-meter accuracy is obtained in an urban canyon. At the same time, VIO shows an accuracy of around 1.5 meters with an accumulating error from the beginning of the flight as GNSS measurements are not available to correct the drift over time.

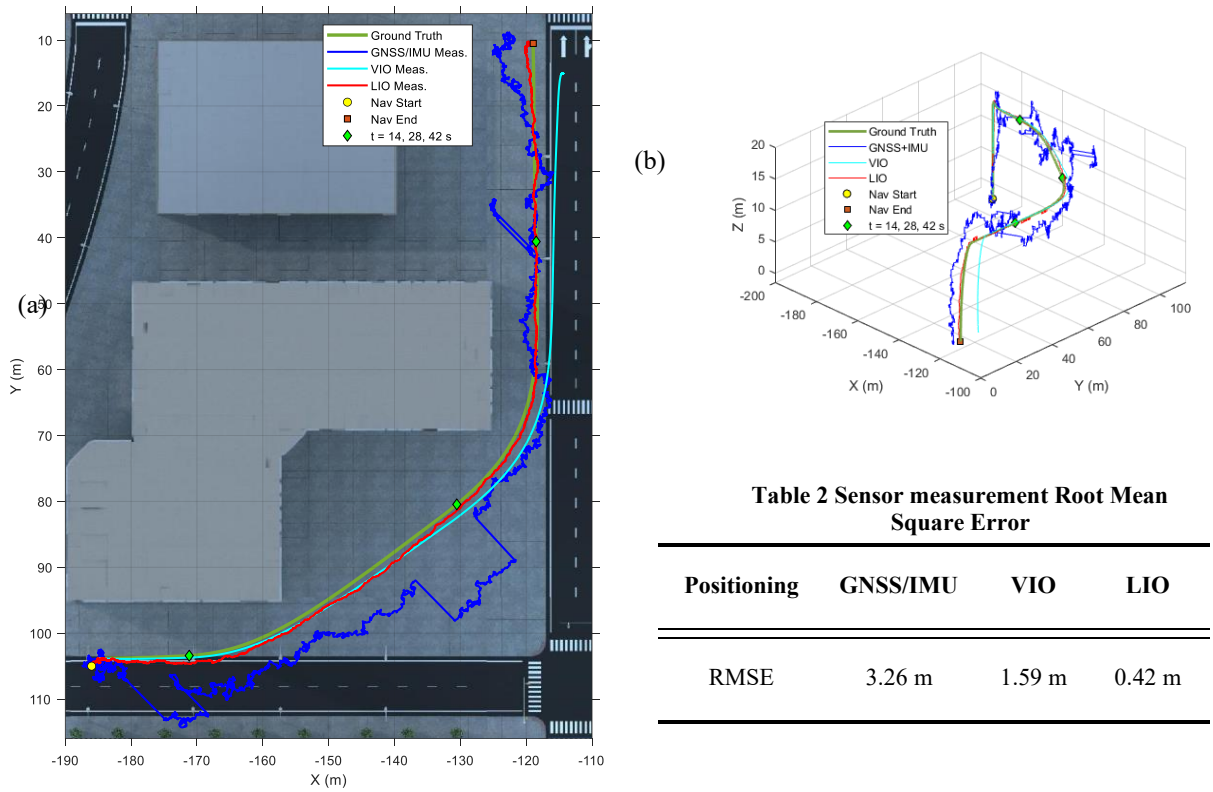


Table 2 Sensor measurement Root Mean Square Error

Positioning	GNSS/IMU	VIO	LIO
RMSE	3.26 m	1.59 m	0.42 m

Figure 4. Simulation results for GNSS/IMU, VIO, and LIO position measurements. Control points are shown at the 25, 50 and 75% of the mission corresponding to 14, 28, and 42 seconds. a) shows the 2D projection of the measurements in the simulation environment, b) the three-dimensional measurements.

E. Fused Position Estimation

Figure 5 (a) illustrates, with a black dotted line, the final positioning estimation, while the interaction between the different sensor model filters in the reinitialization step can be observed to have corrected the VIO and GNSS/IMU position measurement data. It is essential to note from (b) that the mixing weight for VIO is higher at the beginning of the flight when the drift does not pose a risk for the total estimation until before the 10th second, where the drift starts to become noticeable, automatically the system starts the transition from VIO to LIO. The system discarded the GNSS signal despite the initial conditions biased towards the belief of fault-free GNSS with an 80% probability of transition to itself and from other signals. (c) shows the estimated position uncertainty (EPU) of the final position estimation, which is only used as a reference to evaluate the accuracy of the system against a horizontal alert limit of 1 meter, so the system alerts in 1s that the position estimation might have an error out of the sub-meter accuracy threshold.

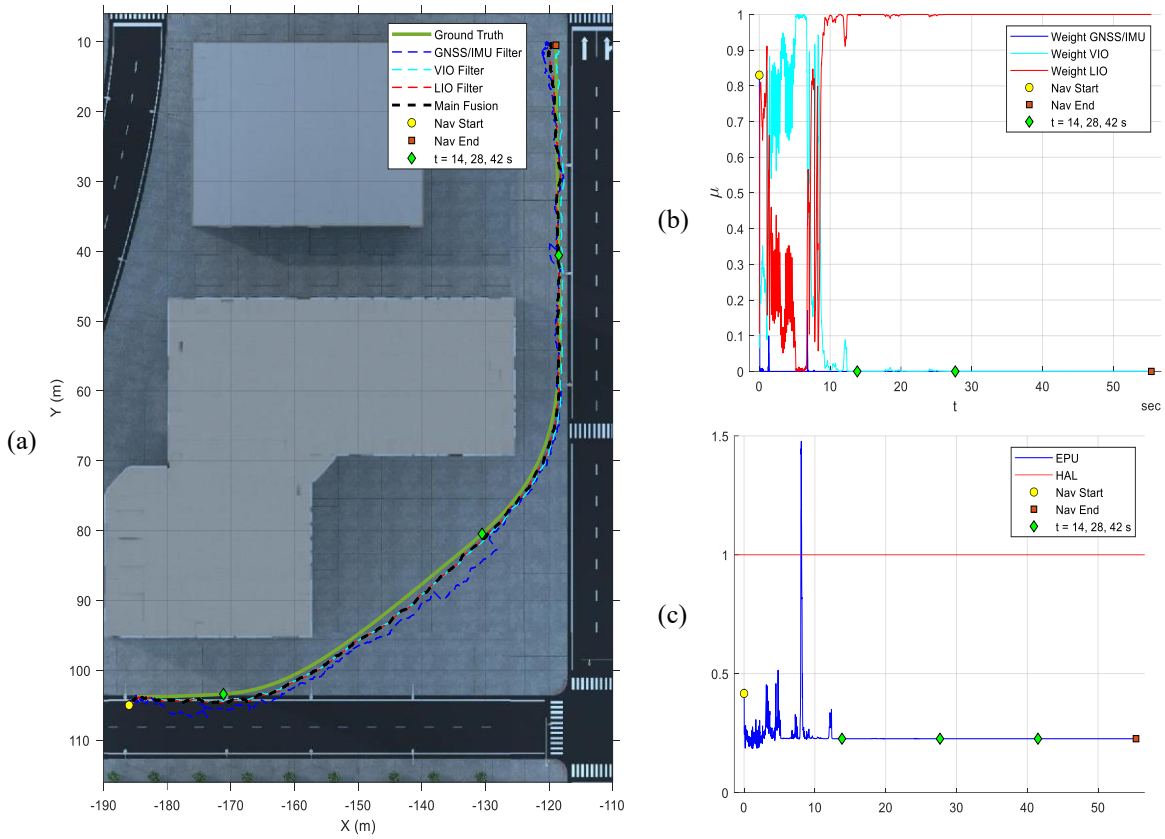


Figure 5. Proposed architecture results where (a) illustrate the overall estimation (black dotted line) and independent full-state Kalman filters (blue, cyan and red dotted lines). (b) shows the mixing weights for the independent filters and (c) the estimated position uncertainty of the overall estimation during the flight.

Figure 6 (a) shows a comparison of the RMSE of individual positioning signals processed with standalone full-state Kalman filters and with the system proposal for the purpose of improvement analysis. It is possible to observe a decrease of 70% in the positioning error measurements after the proposed solution is implemented; see Table 3 for numerical comparison. (b) shows the collection of the individual signals and the final estimation after system implementation, it is possible to observe the similarity between LIO and the main fusion estimation (overall estimation) due to the mixing weight, as seen in Figure 5 (b).

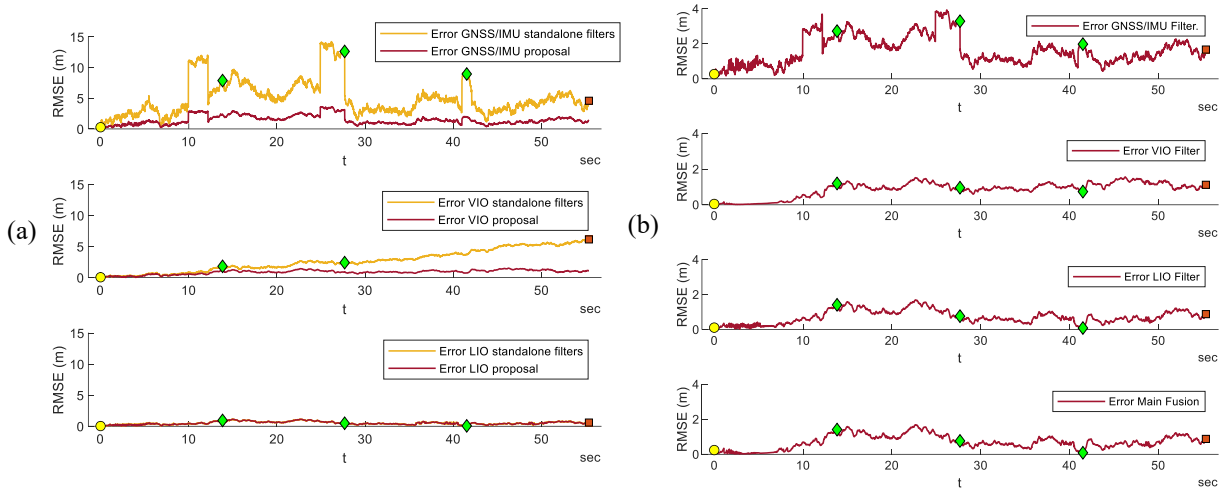


Figure 6. RMSE results, where (a) depicts a comparison between the error of standalone full-state Kalman independent filters for tracking the positioning signals and the full-state Kalman independent filters with the mixing process of the proposed architecture (see eq. (4)) while (b) shows the same three positioning signals from the proposed architecture with a fourth overall estimation composed of the associated weights for each signal (as seen in Figure 5.b)

Table 3 Root Mean Square Error independent filters and the overall estimation

Positioning	RMSE of Independent Filters	RMSE of the Proposed Solution	% Error Reduction
GNSS/IMU	3.25 m	0.99 m	69.5%
VIO	1.60 m	0.49 m	69.5%
LIO	0.43 m	0.42 m	2.5%
Main Fusion	N/A	0.41 m	N/A

F. Failure Modes

Results demonstrate that the estimation of the entire system is automatically adjusted to the signal with the least error at a given time *t*, as seen in the results, suggesting that the methodology can be classified as an autonomous sensor management framework rather than sensor data fusion framework. The overall position estimation is based merely on the weights allocated to each sensor through the process of dynamic uncertainty update, thus obtaining a final estimate which may be composed partially or solely of one or more positioning signals from the independent filters. Some other sensor data fusion solutions make use of a main filter for fusion, as in [17], [18] where the authors implement a federated Kalman filter and particle filter to fuse the positioning data from the available sensors; other options can be the implementation of an EKF, UKF or MSCKF among all its possible variations mentioned in [19]. Recall that after the mixing process for the independent filters from equation (4), according to Table 3, it is possible to reduce the faulty sensors error up to 70%, which can be even higher depending on the fault conditions. Therefore, by substituting the main fusion module with a nonlinear Kalman filter or particle filter, it is feasible to enhance the performance of the individual estimations by obtaining a new estimation that can be better than the rest.

Hence, following the fault categorization in the integrity risk allocation from [20], as it has been stated, the overall estimation is composed of its available signals and can provide an accurate positioning as long as one of the signals is fault-free; hence, the system can mitigate the failure modes:

$$F_i = \{\, GVL \;\; \bar{G}VL \;\; G\bar{V}L \;\; GV\bar{L} \;\; \bar{G}\bar{V}L \;\; \bar{G}V\bar{L} \; G\bar{V}\bar{L} \,\}$$

Where G and $\bar{G}$ indicate GNSS position measurements with and without faults, V and $\bar{V}$, the same situation for VIO and L, $\bar{L}$ for LIO positioning measurements. Then, the system is vulnerable to the case scenario where the failure mode $\bar{G}\bar{V}\bar{L}$ occurs. As a necessary consequence, using an Unscented Kalman Filter is suggested to substitute the main fusion module, fusing the available sensor data that can result in a better estimation than the ones available and eliminate the

dependency on a fault-free signal. The filter can use an IMU model for the filter prediction step and be updated by the available positioning signals as done in [10], thus, enhancing the claimed improvement achieved with the signal mixing process (Table 3).

G. Unsensitivity to definition of Markov chain

The main problem reported by the ISIU methodology is the sensitivity to the Markov chain matrix. The system's performance is highly affected by the information provided in this transition matrix as it provides the priority of transition from one sensor to another. To evaluate the proposal, two different matrices were defined with different values, as done in ISIU results, one with a higher probability of transition to GNSS and the second with a higher probability of transition to LIO. The values of the two matrices are precisely the same as the ones used in ISIU [4] for test replication.

$$p_{ji\,\checkmark} = \begin{matrix} \\ GNSS \\ VIO \\ LIO \end{matrix} \begin{matrix} \begin{matrix} GNSS & VIO & LIO \end{matrix} \\ \begin{bmatrix} 0.90 & 0.03 & 0.07 \\ 0.25 & 0.70 & 0.05 \\ 0.15 & 0.05 & 0.80 \end{bmatrix} \end{matrix} \qquad p_{ji\,\times} = \begin{matrix} \\ GNSS \\ VIO \\ LIO \end{matrix} \begin{matrix} \begin{matrix} GNSS & VIO & LIO \end{matrix} \\ \begin{bmatrix} 0.50 & 0.03 & 0.50 \\ 0.05 & 0.15 & 0.80 \\ 0.05 & 0.30 & 0.65 \end{bmatrix} \end{matrix}$$

Figure 7 (a) shows the mixing process of both cases with the proposed architecture, and (b) illustrates the comparison in the overall estimation error and EPU. Table 4 summarizes the absolute RMSE values; it can be seen that no variation is derived from using different matrix values, and the results remain the same even with different Markov chains. So, it can be concluded that the sensitivity to changes in the Markov chain matrix has been successfully mitigated with the proposed architecture. However, when defining the matrix, the conditions presented in equation (1) must always be followed to fulfill the equality, otherwise, erroneous data can be obtained.

Table 4 Root Mean Square Error for different Markov Chains

Positioning	GNSS/IMU	VIO	LIO	Main Fusion
RMSE p_{ij} ✓	0.993 m	0.488 m	0.419 m	0.416 m
RMSE p_{ij} ×	1.002 m	0.488 m	0.419 m	0.416 m

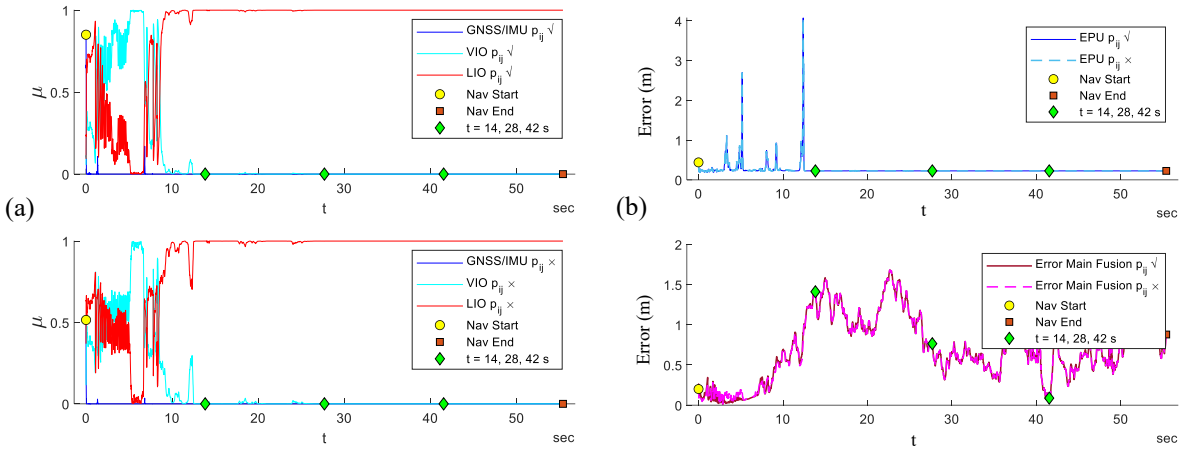


Figure 7. Results comparison with two different transition matrices, (a) showing the mixing weights and (b) the EPU and Main fusion error in meters.

H. Jump Transition Sensitivity

The proposal's primary drawback is the one introduced by the adaptive transition matrix method indicated in IV.C. Because the correction function depends on the gradient of change of the mixing weight, an abrupt step change (or jump) in the signal will result in a more significant gradient of change, which will then cause the transition values to alter proportionally. Then, after a substantial change, as shown in Figure 8 (a), the system switched to VIO despite its

faulty conditions because of a sudden change in LIO caused by simple noise that terminated in a complete signal switch.

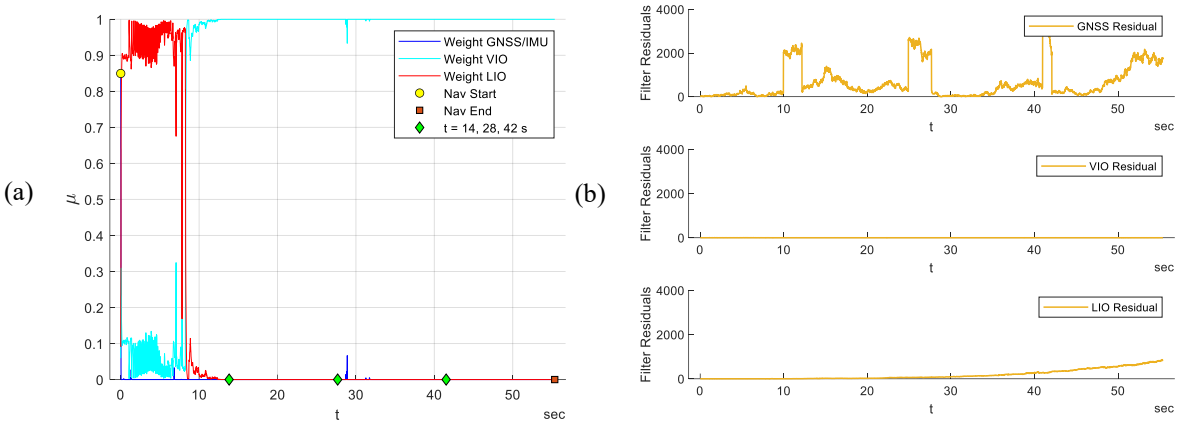


Figure 8. (a) Jump transition flaw from LIO to VIO when a sudden change in the signal is presented. (b) shows the residuals of the independent filters, the value increases proportionally to the faults.

This problem directly compromises the following failure modes:
$F_i = \{\ \bar{G}\bar{V}L\ \ \bar{G}V\bar{L}\ G\bar{V}\bar{L}\ \}$

To address this issue, it is suggested that the correction function's gradient of change be replaced with a function based on the residuals, which will be directly related to the fault and not to changes in the mixing weight, as seen in Figure 8 (b).

$$f_{k/k}^{(i)} = \frac{1}{1-\Delta\mu_{k/k}^{(i)\mathrm{T}}} \rightarrow f_{k/k}^{(i)} = \frac{1}{1-R(t)}$$

VI. Conclusion

This paper aimed to develop an enhanced adaptative sensor switching mechanism for improved robustness in GNSS-degraded environments while accounting for accuracy when one or more sensors face faulty conditions. Previous studies have proposed an integrated multi-sensor fusion architecture that manages faults and excludes them while the integrity is being monitored. However, that architecture depends on the heuristic determination of a fixed transition Markov chain matrix, which must be updated for different sensor conditions and is unsuitable for autonomous systems. For that reason, this paper proposed annexing a new methodology called Dynamic Uncertainty Update to handle the heuristic determination of the transition matrix where the sensor uncertainty is updated by a correction function computed from the current and previous mode transition probabilities to obtain a gradient measure that can be used to estimate the sensor uncertainty. Analysis and results suggest that the methodology can reduce up to 70% of the errors of independent filters of each sensor model. In addition, the results show non-sensitivity to changes in the Markov chain, which previous research reported as the methodology's main problem.

Nevertheless, the proposed architecture shows a drawback adopted from incorporating the mode probability gradient into the correction function to update the Markov chain to the next epoch. This issue can lead to errors when high jumps are encountered in the mixing process for the transition between two sensors. To address this problem, it is proposed to replace the gradient with a function of the residuals from independent filters. Future work will focus on defining the function and testing the architecture on a real-case scenario.

References

[1] Z. M. Kassas, P. Closas, and J. Gross, "Navigation Systems Panel Report Navigation Systems for Autonomous and Semi-Autonomous Vehicles: Current Trends and Future Challenges," *IEEE Aerospace and Electronic Systems Magazine*, vol. 34, no. 5, pp. 82–84, May 2019, doi: 10.1109/MAES.2019.2906971.

[2] S. Bhamidipati and G. X. Gao, "SLAM-based Integrity Monitoring Using GPS and Fish-eye Camera," *Proceedings of the 32nd International Technical Meeting of the Satellite Division of the Institute of Navigation, ION GNSS+ 2019*, pp. 4116–4129, Oct. 2019, doi: 10.48550/arxiv.1910.02165.

[3] Juan D. Jurado, "AUTONOMOUS AND RESILIENT MANAGEMENT OF ALL-SOURCE SENSORS FOR NAVIGATION ASSURANCE AIR FORCE INSTITUTE OF TECHNOLOGY," Air Force Institute of Technology, Ohio, 2019.

[4] Q. Meng and L. T. Hsu, "Resilient Interactive Sensor-Independent-Update Fusion Navigation Method," *IEEE Transactions on Intelligent Transportation Systems*, 2022, doi: 10.1109/TITS.2022.3150273.

[5] Z. Z. Kassas and J. Khalife, "On the Achievability of Submeter-Accurate UAV Navigation with Cellular Signals Exploiting Loose Network Synchronization," *IEEE Trans Aerosp Electron Syst*, pp. 1–1, 2022, doi: 10.1109/TAES.2022.3162770.

[6] J. J. Morales, I. M. Zaher Kassas, and S. Member, "Tightly Coupled Inertial Navigation System With Signals of Opportunity Aiding; Tightly Coupled Inertial Navigation System With Signals of Opportunity Aiding," 2021, doi: 10.1109/TAES.2021.3054067.

[7] A. A. Abdallah and Z. M. Kassas, "UAV Navigation With 5G Carrier Phase Measurements," *Proceedings of the 34th International Technical Meeting of the Satellite Division of the Institute of Navigation, ION GNSS+ 2021*, pp. 3294–3306, Sep. 2021, doi: 10.33012/2021.18101.

[8] Z. Z. M. Kassas, M. Maaref, J. J. Morales, J. J. Khalife, and K. Shamei, "Robust Vehicular Localization and Map Matching in Urban Environments through IMU, GNSS, and Cellular Signals," *IEEE Intelligent Transportation Systems Magazine*, vol. 12, no. 3, pp. 36–52, Sep. 2020, doi: 10.1109/MITS.2020.2994110.

[9] J. Khalife, S. Ragothaman, and Z. M. Kassas, "Pose estimation with lidar odometry and cellular pseudoranges," *IEEE Intelligent Vehicles Symposium, Proceedings*, pp. 1722–1727, Jul. 2017, doi: 10.1109/IVS.2017.7995956.

[10] H. Lu, H. Shen, B. Tian, X. Zhang, Z. Yang, and Q. Zong, "Flight in GPS-denied environment: Autonomous navigation system for micro-aerial vehicle," *Aerosp Sci Technol*, vol. 124, p. 107521, 2022, doi: 10.1016/j.ast.2022.107521.

[11] H. SHEN, Q. ZONG, H. LU, X. ZHANG, B. TIAN, and L. HE, "A distributed approach for lidar-based relative state estimation of multi-UAV in GPS-denied environments," *Chinese Journal of Aeronautics*, vol. 35, no. 1, pp. 59–69, Jan. 2022, doi: 10.1016/J.CJA.2021.04.021.

[12] U.S. Department of Homeland Security, "Report on Positioning, Navigation, and Timing (PNT) Backup and Complementary Capabilities to the Global Positioning System (GPS)," Apr. 2020.

[13] G. Xie, L. Sun, T. Wen, X. Hei, and F. Qian, "Adaptive Transition Probability Matrix-Based Parallel IMM Algorithm," *SYSTEMS*, vol. 51, no. 5, 2021, doi: 10.1109/TSMC.2019.2922305.

[14] X. Bi, J. Du, J. Gao, W. Wang, and Y. Gao, "The IMM tracking algorithm for maneuvering target with adaptive Markov transition probability matrix," *Proceedings of the 2015 10th IEEE Conference on Industrial Electronics and Applications, ICIEA 2015*, pp. 1279–1282, Nov. 2015, doi: 10.1109/ICIEA.2015.7334305.

[15] U. I. Bhatti and W. Y. Ochieng, "Failure modes and models for integrated GPS/INS systems," *Journal of Navigation*, vol. 60, no. 2, pp. 327–348, May 2007, doi: 10.1017/S0373463307004237.

[16] T. Shan, B. Englot, D. Meyers, W. Wang, C. Ratti, and D. Rus, "LIO-SAM: Tightly-coupled Lidar Inertial Odometry via Smoothing and Mapping," *IEEE International Conference on Intelligent Robots and Systems*, pp. 5135–5142, Jul. 2020, doi: 10.48550/arxiv.2007.00258.

[17] D. H. Won *et al.*, "INS/vSLAM system using distributed particle filter," *Int J Control Autom Syst*, vol. 8, no. 6, pp. 1232–1240, Dec. 2010, doi: 10.1007/s12555-010-0608-7.

[18] J. H. Choi, Y. W. Park, J. Kim, T. S. Choe, and J. B. Song, "Federated-filter-based unmanned ground vehicle localization using 3D range registration with digital elevation model in outdoor environments," *J Field Robot*, vol. 29, no. 2, pp. 298–314, Mar. 2012, doi: 10.1002/ROB.21416.

[19] Y. Alkendi, L. Seneviratne, and Y. Zweiri, "State of the Art in Vision-Based Localization Techniques for Autonomous Navigation Systems," *IEEE Access*, vol. 9, pp. 76847–76874, 2021, doi: 10.1109/ACCESS.2021.3082778.

[20] H. Jiang, T. Li, D. Song, and C. Shi, “An Effective Integrity Monitoring Scheme for GNSS/INS/Vision Integration Based on Error State EKF Model,” *IEEE Sens J*, vol. 22, no. 7, pp. 7063–7073, Apr. 2022, doi: 10.1109/JSEN.2022.3154054.



https://dspace.org/

Robust multi-sensor navigation in GNSS degraded environments

Villalobos Hernandez, Guillermo E.; Petrunin, Ivan; Shin, Hyo-Sang; Gilmour, James

2023-01-19
American Institute of Aeronautics and Astronautics (AIAA)
https://doi.org/10.2514/6.2023-2242
Villalobos Hernandez GE, Petrunin I, Shin H-S, Gilmour J. (2023) Robust multi-sensor navigation in GNSS degraded environments. In: AIAA SciTech Forum 2023, 23-27 January 2023, National Harbor, Maryland, USA. Paper number AIAA 2023-2242

Downloaded from a DSpace repository. https://dspace.org/